Received: 22 November 2019 | Revised: 22 December 2019 | Accepted: 22 December 2019

DOI: 10.1111/jace.16998

SPECIAL ISSUE ARTICLE

Journal of the American Ceramic Society

Structure and lithium-ion mobility in $Li_{1.5}M_{0.5}Ge_{1.5}(PO_4)_3$ (M = Ga, Sc, Y) NASICON glass-ceramics

Igor d'Anciães Almeida Silva[1] | **Adriana M. Nieto-Muñoz**[2] | **Ana Candida M. Rodrigues**[3] | **Hellmut Eckert**[1,4]

[1]São Carlos Institute of Physics, São Paulo University, São Carlos, Brazil

[2]Programa de Pós-Graduação em Ciência e Engenharia de Materiais, Universidade Federal de São Carlos, São Carlos, Brazil

[3]Departamento de Engenharia de Materiais, Universidade Federal de São Carlos, São Carlos, Brazil

[4]Institut für Physikalische Chemie, WWU Münster, Münster, Germany

Correspondence
Hellmut Eckert, São Carlos Institute of Physics, São Paulo University, 13566-590, São Carlos, SP, Brazil
Email: eckerth@uni-muenster.de

Funding information
Fundação de Amparo à Pesquisa do Estado de São Paulo, Grant/Award Number: 2013/07793-6

Abstract

This work reports structural and lithium-ion mobility studies in NASICON single- or multiple phase $Li_{1+x}M_xGe_{2-x}(PO_4)_3$ ($M = Ga^{3+}$, Sc^{3+}, Y^{3+}) glass-ceramics using solid-state NMR techniques, X-ray powder diffraction, and impedance spectroscopy. X-ray powder diffraction data show the successful incorporation of Ga^{3+} and Sc^{3+} into the Ge^{4+} octahedral sites of the NASICON structure at the levels of $x = 0.5$ and 0.4, respectively. The glass-to-crystal transition was further characterized by multinuclear NMR and electrical conductivity measurements. Among the studied samples, the gallium-containing glass-ceramic presented the highest DC conductivity, 1.1×10^{-4} S/cm at room temperature, whereas for the Sc-containing samples, the maximum room temperature conductivity that could be reached was 4.8×10^{-6} S/cm. No indications of any substitution of Ge^{4+} by Y^{3+} could be found.

KEYWORDS

ionic conductivity, nuclear magnetic resonance, phosphates, structure

1 | INTRODUCTION

Lithium-ion batteries played such an important role in the technological revolution that took place in the past two decades that their developers received the 2019 Nobel Prize in Chemistry.[1] To date, commercial lithium-ion batteries employ liquid-organic electrolytes which present both operational drawbacks like restricted cyclability (due to electrode corrosion) and health hazards caused by leakage of the electrode.[2–5] All-solid-state batteries are believed to be the next step in the evolution of batteries as they avoid such drawbacks.[2–5] Therefore, optimized solid-state electrolytes with high ionic conductivity are required. One of the most promising solid electrolyte systems found in the literature is based on glass-ceramics in the Na-Super Ionic Conductor (NASICON) phase field.[2,3] The first NASICON glass-ceramic systems were reported and patented by J. Fu in 1997.[6–9] Typical compositions are $Li_{1+x}Al_xM_{2-x}(PO_4)_3$, and $Li_{1+x+y}Al_yM_{2-y}Si_xP_{3-x}O_{12}$ systems where M = Ti and Ge. In the NASICON structure, tetravalent M ions are octahedrally bonded by corner-sharing oxygens to phosphate tetrahedra. Li^+ ions can occupy two sites named M1 (sixfold coordinated located between MO_6 octahedra) and M2 (eightfold coordinated and located between two MO_6 columns). In the $LiGe_2(PO_4)_3$ parent compound, the M1 sites are fully occupied while the M2 sites are vacant, and at elevated temperatures, ionic transport occurs by hopping between these sites.[2,3,10] To improve the ionic conduction, aliovalent substitution of M^{4+} by M'^{3+} ions having slightly larger ionic radii[11] than M^{4+} can be employed. This procedure widens the bottleneck window

between the two sites and introduces additional Li^+ ions in the NASICON structure for charge compensation, which can be accommodated at the M2 sites. At higher x contents, a redistribution of populations takes place.[2,3]

In the last years, a large number of studies have focused on the $Li_{1+x}Al_xGe_{2-x}(PO_4)_3$ system characterizing structural aspects and lithium-ion mobility[12–17] as well as technological applications.[18–20] Further compositional optimization has been attempted by combining isovalent (Sn^{4+} and Ti^{4+}) and aliovalent substitution (Al^{3+} and Cr^{3+}) approaches[21–23] in an effort to decrease the activation energy of M1 → M2 hopping. Aliovalent substitution by trivalent ions that are substantially larger than Ge^{4+} has been rarely reported in $LiGe_2(PO_4)_3$ glass-ceramics, apart from the most recent work of by Zhang et al.[24] reporting successful substitution of Ge^{4+} by Ga^{3+}. Here we are reporting the results of our recent efforts of substituting Ge^{4+} by Ga^{3+}, Sc^{3+}, and Y^{3+} in $LiGe_2(PO_4)_3$–based NASICON glass-ceramics probed by X-ray powder diffraction, impedance spectroscopy, and solid-state NMR. Such substitutions have been recently studied for the analogous $LiTi_2(PO_4)_3$ glass-ceramics[25] and (unsuccessful) yttrium substitution was attempted in $LiGe_2(PO_4)_3$ by the solid-state reaction.[26]

2 | EXPERIMENTAL PROCEDURES

Stoichiometric mixtures of Li_2CO_3 (Vetec, 99%), GeO_2 (Sigma, 99.99%), $NH_4H_2PO_4$ (Sigma, ≥98%), Ga_2O_3 (ABCR, 99.99%), Sc_2O_3 (ABCR, 99.9%), and Y_2O_3 (REEtec, 99.9941%) were used to synthesize the glass precursors. Raw materials were heated at 700°C for 2 hours to eliminate water, CO_2, and to decompose the ammonium dihydrogen phosphate. The mixtures were then melted at 1200°C for 2 hours in a platinum-gold crucible, quenched in a cylindrical mold and annealed at 450°C for 2 hours to relieve thermal stress. The resulting glasses were sliced into 3.0 mm thick discs. Glass transition onset (T_g) and crystallization peak (T_p) temperatures were determined by DSC analysis (Netzsch DSC404) applying a heating rate of 10°C/min. The results are summarized in Figure 1 and Table 1. Fully crystallized samples were produced by heat treatment of the precursor glasses at the crystallization temperature for 3 hours. For $Li_{1.5}Ga_{0.5}Ge_{1.5}(PO_4)_3$ precursor glass (LGGP), heat treatment was employed at 606°C for 3 hours and the resulting crystallized sample was labeled LGGP-C-606. For $Li_{1.5}Sc_{0.5}Ge_{1.5}(PO_4)_3$ precursor glass (LSGP), heat treatments were done on separate samples at 600°C for 1 hour, 690°C for 1 hour, and 832°C for 3 hours. Labels are LSGP-C-600, LSGP-C-690, and LSGP-C-832, respectively. Finally, for $Li_{1.5}Y_{0.5}Ge_{1.5}(PO_4)_3$ precursor glass (LYGP), heat treatment was performed at 728°C for 3 hours and the crystallized sample was labeled LYGP-C-728.

X-ray powder diffraction patterns at room temperature were taken for all synthesized samples in a Rigaku Ultima IV X-ray diffractometer operating with Cu K_α radiation between 5° and 100° in steps of 0.02°. An integrator time of 1 second was used. Rietveld refinements of the experimental powder patterns were done using the software MAUD to acquire the lattice parameters, the volume of the unit cell, and the ratios of the crystallized phases.[27] The refinements assume an $R\bar{3}c$ space group.

Impedance spectroscopy was performed in a Novocontrol Alpha Analyzer coupled with a Novotherm furnace, operating at temperatures between 30°C and 140°C (accuracy: ±0.1°C) in the

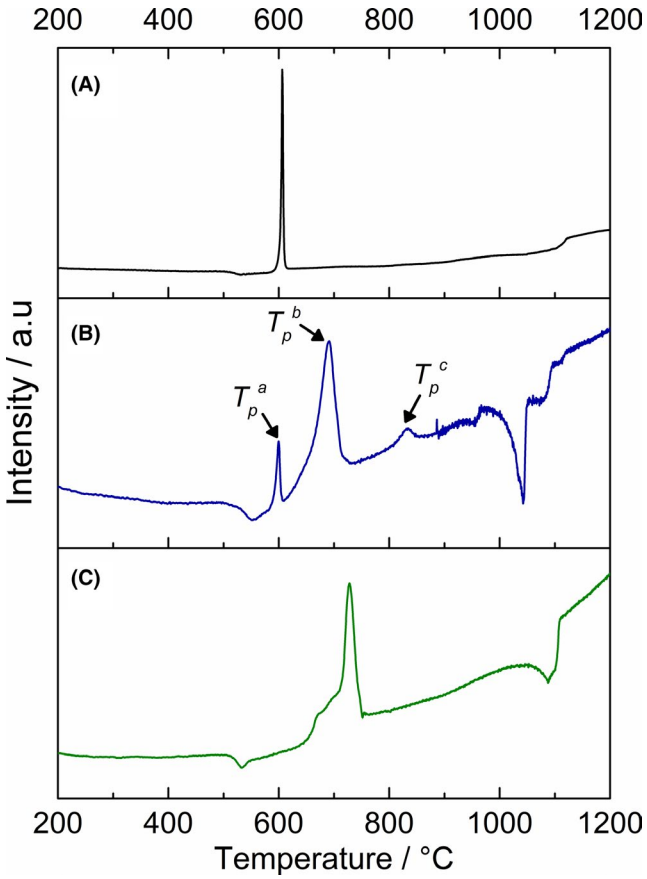

FIGURE 1 DSC thermograms of LGGP (A), LSGP (B), and LYGP (C) precursor glasses. Glass transition temperatures (T_g) and crystallization peak temperatures (T_p) are listed in Table 1. Thermograph A shows that LGGP precursor glass crystallizes only one phase while LSGP and LYGP precursor glasses crystallize more than one phase. [Color figure can be viewed at wileyonlinelibrary.com]

TABLE 1 Glass transition temperature (T_g) and crystallization temperature (T_p) acquired from the DSC thermograms in Figure 1. Estimated errors are 2°C

Sample	T_g /°C	T_p /°C
LGGP	506	606
LSGP	515	600[a]/690[b]/832[c]
LYGP	510	728

[a]First exothermal peak.

[b]Second exothermal peak.

[c]Third exothermal peak.

10^7-0.1 Hz frequency range. Voltage amplitudes of 300 mV were applied. For these electrical measurements, parallel surfaces of glass-ceramics were previously sputtered with gold during 300 seconds. Total ionic conductivity data (σ) was calculated from

$$\sigma = \frac{L}{RA}, \quad (1)$$

where L is the sample thickness (around 3 mm) and A is the area of the electrode in contact with the sample. R is the total resistance acquired from the Z' vs Z'' impedance plots using the WinFIT software.

High-resolution ^{31}P, ^{71}Ga, and ^{45}Sc NMR spectra were measured in a Bruker Avance 600 spectrometer operating at 14.1 T under Magic Angle Spinning (MAS) conditions. Single-pulse ^{31}P (resonance frequency: 243.04 MHz) MAS NMR experiments were taken for all samples in a commercial triple channel 3.2 mm probe operating at a spinning speed of 20.0 kHz. A 3.0 μs pulse length and a recycle delay of 90 seconds were employed. Chemical shift values were referenced against 85% H_3PO_4 using powdered BPO_4 (−29.27 ppm) as a secondary standard. Single-pulse ^{45}Sc (resonance frequency: 145.84 MHz) and ^{71}Ga (resonance frequency: 183.15 MHz) MAS NMR experiments were performed in a commercial triple channel 2.5 mm probe with spinning speeds of 20.0 kHz for ^{45}Sc and 10.0 kHz and 45.0 kHz for ^{71}Ga (in the latter case, a 1.3 mm probe was used). A pulse length of 0.6 μs and a recycle delay of 4 seconds were used for ^{45}Sc experiments while pulse lengths of 0.5 and 0.775 μs with recycle delays of 20 seconds and 1 second were used for the 10.0 and 45.0 kHz ^{71}Ga NMR experiments, respectively. ^{71}Ga QCPMG (Quadrupolar Carr-Purcell-Meiboom-Gill) experiments were done for LGGP precursor glass and its glass-ceramic (sample LGGP-C-606), using the pulse sequence of Larsen et al.[28] Pulse widths of 0.75 and 1.5 μs (30° and 60° flip angles, respectively), a nutation frequency of 111 kHz, and a recycle delay of 0.1 seconds were used. For these experiments, 150 echoes were acquired with 5×10^5 scans. Chemical shifts were referenced to powdered $ScPO_4$ (−48.2 ppm[29] against 1 mol/L $ScCl_3$ solution) and GaP (307 ppm[30] against 1 mol/L $Ga(NO_3)_3$ solution), respectively.

Static ^{7}Li NMR experiments were done in an Agilent DD2 600 MHz spectrometer interfaced with a 5.6 T magnet using a commercial triple channel 4 mm probe between 160 K and 440 K. Single-pulse experiments employed pulse lengths of 1 μs with relaxation delays between 0.1 and 60 seconds. Chemical shifts were referenced to a 1 mol/L LiCl solution. Experimental spectra were analyzed using Gaussian and/or Lorentzian line shapes to extract the full width at half maximum of the spectra. All data processing and parameter extraction was done using DMFIT software.[31]

3 | RESULTS

3.1 | Structure

X-ray powder patterns of all the precursor glasses (Figure 2) present no sharp diffraction peaks while the patterns for the crystallized samples (Figure 3) present peaks related to crystalline $LiGe_2(PO_4)_3$ (PDF2 card number 80-1922) indicating the crystallization of a NASICON phase. Phase-pure NASICON materials were only obtained for the gallium-substituted compound, except for a small unidentified peak near $2\theta = 17°$ for the sample LGGP-C-606. For crystallized samples containing scandium, X-ray diffraction patterns showed that the sample LSGP-C-600 (Figure 3) is still in the glassy state. The LSGP-C-690 sample showed a dominantly crystallized NASICON phase while sample LSGP-C-832 showed multiple phases, including $LiScP_2O_7$ (PDF2 card number 47-931) and GeO_2 (PDF2 card number 85-1515). Finally, peaks assigned to YPO_4 (PFD2 card number 83-658) and $Li_4P_2O_7$ (PDF2 card number 3-222) were identified in the X-ray powder pattern of sample LYGP-C-728. Table 2 lists the lattice constants, unit cell volumes, and percentages of the crystalline NASICON phases determined by Rietveld refinements (Figure 3) as well as for pristine $LiGe_2(PO_4)_3$ NASICON.[31] Approximate mass fractions of the other crystalline phases as deduced from XRD are (30.7 ± 0.2)% for $LiScP_2O_7$; (5.7 ± 0.2)% for GeO_2; (23.0 ± 0.2)% for YPO_4 and (2.8 ± 0.2)% for $Li_4P_2O_7$. The data shown in Table 2 for the LYGP-C-728 sample is in good agreement with those reported for the nominal $Li_{1.4}Y_{0.4}Ge_{1.6}(PO_4)_3$ synthesized by the solid-state reaction.[26]

^{31}P MAS NMR spectra of samples LGGP and LGGP-C-606 are displayed in Figure 4. For the precursor glass, a broad

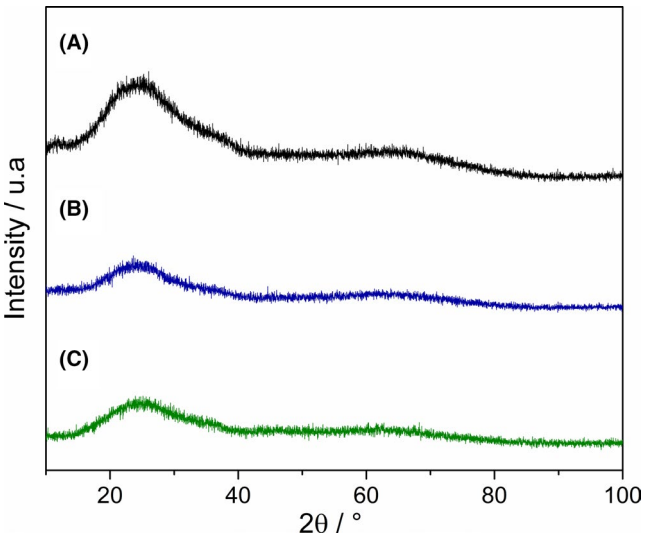

FIGURE 2 X-ray powder patterns for LGGP (A), LSGP (B), and LYGP (C) precursor glasses. These patterns show that all samples are indeed in the glassy state. [Color figure can be viewed at wileyonlinelibrary.com]

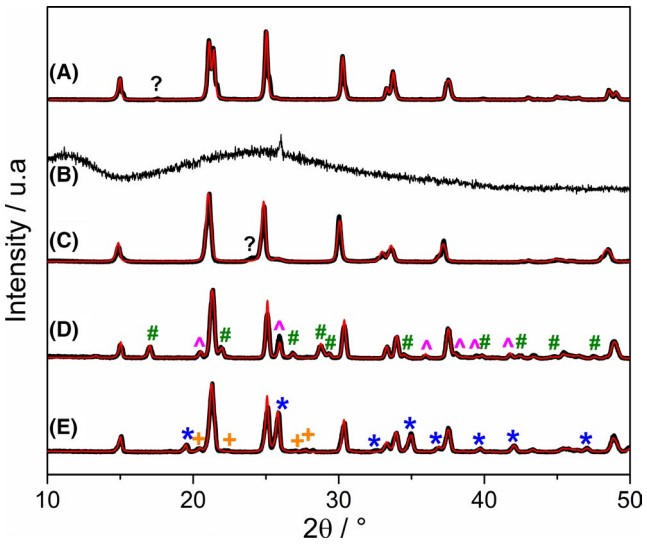

FIGURE 3 X-ray powder patterns of samples LGGP-C-606 (A), LSGP-C-600 (B), LSGP-C-690 (C), LSGP-C-832 (D), and LYGP-C-728 (E). Symbols refer to unknown peaks (?), $LiScP_2O_7$ (#), GeO_2 (^), YPO_4 (*), and $Li_4P_2O_7$ (+). Unmarked peaks are attributed to NASICON phases. Rietveld refinements (red lines) of the experimental X-ray diffraction patterns (black curves) were done considering the intended substitution for samples LGGP-C-606 and LSGP-C-690. For samples LSGP-C-832 and LYGP-C-728, the refinements take into account a $LiGe_2(PO_4)_3$ NASICON phase. Pattern B shows that sample LSGP-C-600 remains in the glass phase after heat treatment of one hour at 600°C. Patterns C and D show that samples LSGP-C-832 and LTGP-C-728 crystallize more phases alongside a $LiGe_2(PO_4)_3$ NASICON phase. [Color figure can be viewed at wileyonlinelibrary.com]

resonance line around −25 ppm is observed, reflecting phosphorus environments dominated by two bridging oxygen species in the glass phase (P^2 units). For the crystallized samples, however, the spectra are characterized by sharp resonance lines. Table 3 summarizes the results of the spectral deconvolutions conducted. The LGGP-C-606 sample exhibits a typical spectrum expected for statistical substitution of Ge^{4+} by Ga^{3+} with partially resolved contributions from $P^4_{4Ge,0Ga}$, $P^4_{3Ge,1Ga}$, $P^4_{2Ge,2Ga}$, and $P^4_{1Ge,3Ga}$ units.[24] In contrast to reference 24, no $GaPO_4$ impurities were observed at the $x = 0.5$ substitution level.

Figure 5 shows the ^{31}P MAS NMR spectra of the scandium-containing samples. Precursor glass (LSGP) and sample LSGP-C-600 present a broad resonance like the LGGP sample. The spectrum of sample LSGP-C-690 contains features related to the substitution of Ge^{4+} by Sc^{3+} in the NASICON structure. In this case, numerical deconvolution of the spectrum was able to identify $P^4_{4Ge,0Sc}$, $P^4_{3Ge,1Sc}$, and $P^4_{2Ge,2Sc}$ units as well as a major broad feature assigned to ^{31}P nuclei in a residual glassy phase. For sample LSGP-C-832, the NASICON signal attributed to the $P^4_{4Ge,0Sc}$ sites at −44.9 ppm is accompanied by various unassigned resonances (P1-P2, see Table 3) and one at −15 ppm due to $LiScP_2O_7$.[33] P2 may be assigned to P^2 units (phosphate units with two bridging oxygens) in $[Sc(PO_3)_3]_n$ polyphosphate chains.[34]

Figure 6 presents the ^{31}P MAS NMR spectra of samples LYGP and LYGP-C-728. While the precursor glass only produces a broad signal, the spectrum of sample LYGP-C-728 consists of three prominent resonances: two overlapping signals at −45.2 and −44.1 ppm may be assigned to $P^4_{4Ge,0Y}$ phosphate units[13,35] whereas the one at −12.8 ppm belongs to YPO_4. There is no indication of Ge^{4+}-> Y^{3+} substitution. Finally, the ^{31}P MAS NMR spectra of samples LGGP-C-606, LSGP-C-832, and LYGP-C-728 present two signals above −10 ppm which can be ascribed to the two P^1 units of $Li_4P_2O_7$.

Figure 7 and Table 4 summarize the ^{45}Sc MAS NMR results. For the precursor glass, a broad asymmetric resonance at 11.6 ppm with a large average quadrupole coupling constant C_Q of 12.5 MHz dominates the spectrum. This signal was simulated using the Czjzek model, which is based on a distribution of chemical shifts and quadrupolar coupling constants (C_Q).[36] This resonance is related to ^{45}Sc nuclei dispersed in the glass matrix. A resonance at −42.6 ppm is also observed with low intensity. Similar resonances appear in the spectrum of sample LSGP-C-600 but at 8.7 and −55.0 ppm, respectively. For sample LSGP-C-690, only an asymmetric signal is observed at 43.3 ppm, which is attributed to the six-coordinate Sc atoms on the Ge sites in the NASICON structure Finally, the ^{45}Sc MAS

TABLE 2 Lattice constants (a, b, and c), unit cell volume, and fraction of the NASICON crystalline phases found by Rietveld refinement of the X-ray powder patters of the crystalline samples. Estimated errors are 0.002 Å for lattice constants, 0.1 $Å^3$ for the unit cell volume, and 0.2% for fraction. Refinements for samples LSGP-C-832 and LYGP-C-728 assume a $LiGe_2(PO_4)_3$ NASICON phase while the refinements for samples LGGP-C-606 and LSGP-C-690 assume substitution of Ge^{4+} by Ga^{3+} and Sc^{3+}, respectively

Sample	Fraction /%	$a = b$/Å	c/Å	V/$Å^3$	References
$LiGe_2(PO_4)_3$		8.275	20.470	1213.9	32
$LiGe_2(PO_4)_3$		8.2829	20.501	1218.1	26
$LiGe_2(PO_4)_3$		8.2501	20.5870	1213.5*	21
$LiGe_2(PO_4)_3$		8.263	20.491	1211.8	24
$Li_{1.4}Ga_{0.4}Ge_{1.6}(PO_4)_3$		8.281	20.542	1219.8	24
LGGP-C-606	100	8.276	20.587	1221.1	This work
LSGP-C-690	100	8.359	20.754	1255.8	This work
LSGP-C-832	63.6	8.283	20.502	1218.1	This work
LYGP-C-728	74.2	8.286	20.533	1220.8	This work

*Calculated from the values given in the reference for a and c.

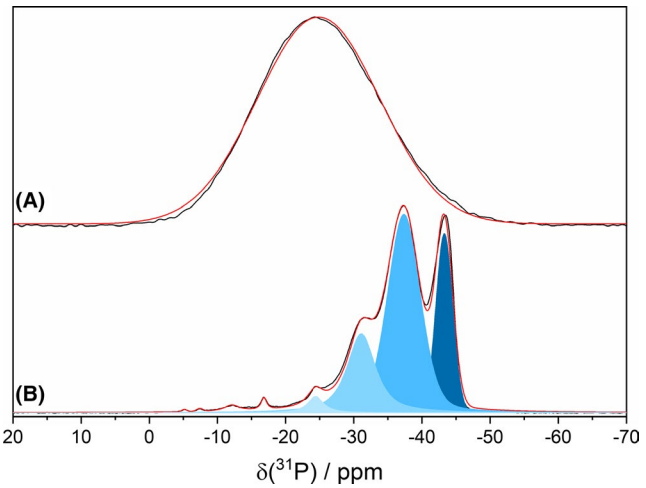

FIGURE 4 ^{31}P MAS NMR spectra of samples LGGP (A) and LGGP-C-606 (B). Black curves are the experimental data and red curves show the simulations. At (B), $P^4_{(4-n)Ge,nGa}$ units are highlighted in shades of blue and correspond to $P^4_{4Ge,0Ga}$, $P^4_{3Ge,1Ga}$, $P^4_{2Ge,2Ga}$, and $P^4_{1Ge,3Ga}$ following the increase of the ppm scale (from dark to light blue). [Color figure can be viewed at wileyonlinelibrary.com]

NMR signals for sample LSGP-C-832 were deconvoluted into four components (Table 4), reflecting the effects of the first- and second-order quadrupolar perturbations on the Zeeman levels.

^{71}Ga MAS NMR experiments were attempted for both LGGP and LGGP-C samples at MAS speeds of 45 and 10 kHz, respectively (Figure 8). Three resonances were observed in the spectrum of sample LGGP at 106.9, 21.4, and −38.6 ppm. These signals were assigned to four-, five-, and six-coordinated gallium species and described by the Czjzek model; in addition ^{71}Ga{^{31}P} rotational echo double resonance results conducted in reference 24 show that all of these species have Ga-O-P connectivity. For sample LGGP-C-606, two resonances at 143.6 ppm and −3.5 ppm were observed and described by the Czjzek model. The first one can be ascribed to the four-coordinated gallium while the latter is assigned to the six-coordinated gallium, which is expected for Ga^{3+} substituting Ge^{4+} in the NASICON structure.[24] This assignment was also proven by ^{71}Ga{^{31}P} REDOR experiments.[24] The content of the five-coordinate gallium is rather low. Deconvolution of the spectrum also showed that the six-coordinated gallium has a larger average quadrupolar coupling constant (C_Q = 3.6 MHz) than the four-coordinated gallium species (C_Q = 1.7 MHz). Table 5 summarizes the results obtained by the deconvolution of the experimental ^{71}Ga MAS NMR spectrum. ^{71}Ga static QCPMG experiments were performed for both LGGP and LGGP-C-606 samples (Figure 8). From the spectra shown in Figure 8, one can see that the precursor glass gives rise to a very broad spikelet pattern centered at around 100 ppm. Its overall spread in frequencies is consistent with the MAS-NMR spectrum indicating that the MAS NMR spectrum is representative of the entire Ga inventory and there is no broad ^{71}Ga signal component that would go undetected in the MAS-NMR spectrum. This spectrum resembles the wideband uniform-rate smooth truncation QCPMG (WURST-QCPMG) spectrum of the model compound β-Ga_2O_3, which also contains four- and six-coordinated gallium atoms.[37,38]

TABLE 3 ^{31}P chemical shift values found by numerical deconvolution of the experimental ^{31}P MAS NMR spectra. Sites generically labeled were not assignable with certainty. $P^4_{4Ge,0M}$ indicates the highly crystalline pristine $LiGe_2(PO_4)_3$ NASICON phase. Estimated errors are 0.2% for the fractions, 0.1 ppm for δ_{iso}, and 3 Hz for the linewidths

Sample	Site	Fraction/%	δ_{iso}/ppm	Linewidth/Hz
LGGP	—	100	−24.8	5160
LGGP-C-606	$P^4_{4Ge,0Ga}$	21.7	−43.3	715
	$P^4_{3Ge,1Ga}$	51.9	−37.3	1380
	$P^4_{2Ge,2Ga}$	21.9	−31.1	1195
	$P^4_{1Ge,3Ga}$	2.8	−24.4	683
	P1	1.0	−12.1	638
	P2	0.7	−16.8	239
	$Li_4P_2O_7$	0.1	−7.4	227
	$Li_4P_2O_7$	0.1	−5.1	204
LSGP	—	100	−25.6	4830
LSGP-C-600	—	100	−23.6	1947
LSGP-C-690	$P^4_{4Ge,0Sc}$	20.9	−41.9	402
	$P^4_{3Ge,1Sc}$	49.1	−37.8	864
	$P^4_{2Ge,2Sc}$	3.0	−27.7	403
	P^2_{glass}	27.1	−25.3	1257
LSGP-C-832	$P^4_{4Ge,0Sc}$	40.3	−44.9	233
	$P^4_{4Ge,0Sc}$	24.4	−45.0	66
	P1	15.0	−24.6	283
	$LiScP_2O_7$	14.9	−15.0	184
	$P^4_{3Ge,1Sc}$	2.7	−38.0	239
	$Li_4P_2O_7$	2.1	−7.5	118
	$Li_4P_2O_7$	1.7	−6.4	111
	P2	0.8	−39.3	165
LYGP	—	100	−23.3	4770
LYGP-C-728	$P^4_{4Ge,0Y}$	51.9	−45.2	98
	$P^4_{4Ge,0Y}$	24.7	−44.1	581
	YPO_4	13.6	−12.8	100
	$Li_4P_2O_7$	4.9	−7.6	125
	$Li_4P_2O_7$	4.6	−5.5	121

3.2 | Lithium-ion dynamics

Lithium-ion dynamics were characterized by impedance spectroscopy and variable-temperature static ^{7}Li NMR for the crystallized samples. Figure 9 shows a representative complex

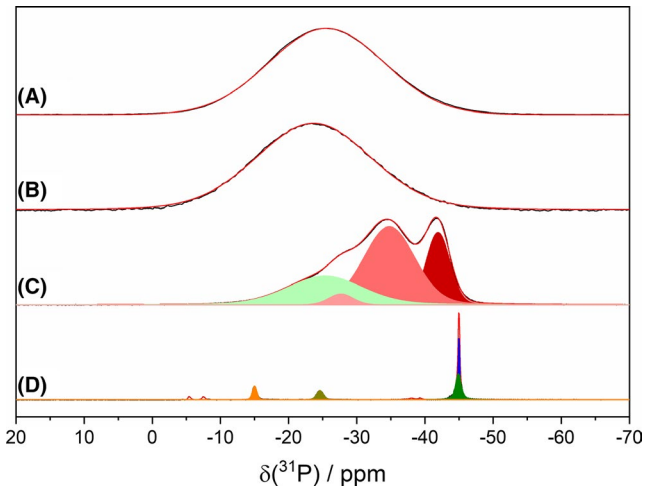

FIGURE 5 ^{31}P MAS NMR spectra of samples LSGP (A), LSGP-C-600 (B), LSGP-C-690 (C), and LSGP-C-832 (D). Black curves are the experimental data and red curves show the simulated spectra. At (C), $P^4_{(4-n)Ge,nSc}$ units are highlighted in shades of red following the increase in ppm scale (from dark to light red) while light green represents the fraction of phosphate units still in glass phase. Unfilled curves are assigned to P1 units in $Li_4P_2O_7$ (phosphate units with only one bridging oxygen) (in D) and the filled orange curve represents the P^4_{4Sc} phosphate units of $LiScP_2O_7$. [Color figure can be viewed at wileyonlinelibrary.com]

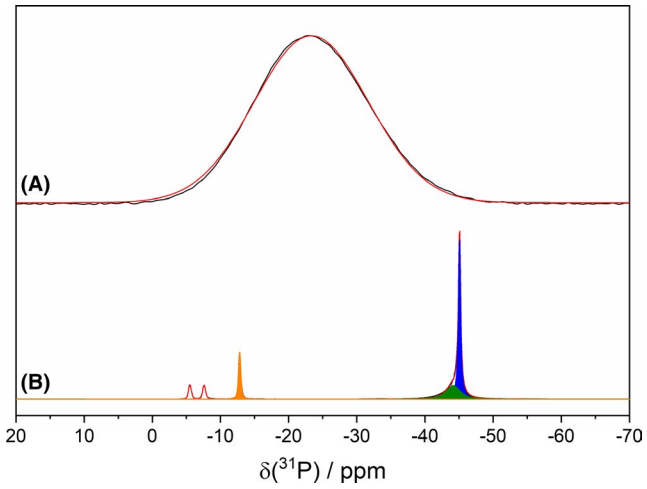

FIGURE 6 ^{31}P MAS NMR spectra of samples LYGP (A) and LYGP-C-728 (B). At (B), different phosphate units are highlighted in blue (highly crystalline $P^4_{4Ge,0Y}$), green ($P^4_{4Ge,0Y}$), and orange (YPO_4). Unfilled curves are assigned to P1 units in $Li_4P_2O_7$ (phosphate units with only one bridging oxygen). Red curves represent simulated spectra. [Color figure can be viewed at wileyonlinelibrary.com]

impedance plot of Ge-substituted glass-ceramics. Note that the semicircles corresponding to samples LSGP-C-832 and LYGP-C-728 are highly flattened, indicating at least two electrical contributions attributed to grain and grain boundary, which are strongly overlapped. Those samples are highly resistive at 40°C, note the intercept of the semicircle with the *x*-axis on the

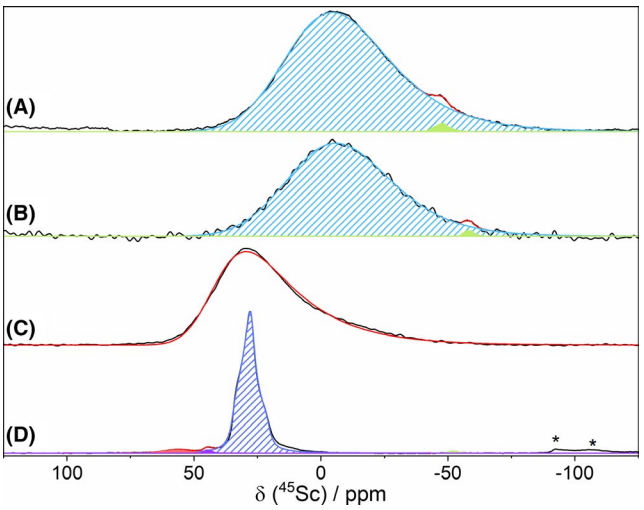

FIGURE 7 ^{45}Sc MAS NMR experimental spectra (black line) and its numerical deconvolutions (red lines) for samples LSGP (A), LSGP-C-600 (B), LSGP-C-690 (C), and LSGP-C-832 (D). Highlighted curves represent different scandium sites as listed in Table 4. [Color figure can be viewed at wileyonlinelibrary.com]

10^6 Ω.cm scale. The inset of Figure 9 shows an incomplete semicircle at the left side for sample LGGP-C-606, indicating the need for employing frequencies higher than 10^7 Hz, which are outside the experimental limits of the equipment. This sample also exhibits the lowest resistivity, note that the *x*-axis´ scale is within the 10^3 Ω.cm range. In all cases, it was not possible to separate grain and grain boundary contributions. Therefore, the discussion of electrical conductivity is limited to the total conductivity of samples, which includes grain and grain boundary contributions. Temperature-dependent σ values were analyzed assuming an Arrhenius behavior (Figure 10) ($\sigma = \sigma_0 \exp\{-E_a/k_B T\}$) and the values for the activation energy (E_a), ionic conductivity at room temperature (σ_{RT}), and the pre-exponential constant (σ_0) are summarized in Table 5. The gallium-containing sample LGGP-C-606 shows the highest total ionic conductivity at room temperature among the analyzed samples (1.1×10^{-4} S/cm) and the lowest activation energy. Conductivities of the other analyzed samples are several orders of magnitude lower. Sample LSGP-C-600, which remained essentially in the glassy state, shows the lowest ionic conductivity at room temperature, 7.9×10^{-11} S/cm (Table 6).

In order to probe the lithium mobility at the local level in our samples in more detail, temperature-dependent ^{7}Li NMR experiments (between 160 and 440 K) were measured under static conditions for LGGP-C-606, LSGP-C-690, LSGP-C-832, and LYGP-C-728 glass-ceramics (see Figure 11 for the representative case of LGGP-C-606). The temperature dependence of the full width at half maximum (FWHM) of the curves is plotted in Figure 12. For the samples containing scandium and yttrium, one can see the typical behavior of motional narrowing, where the FWHM is almost constant at low temperature (rigid lattice regime) and rapidly decreases above an onset temperature T_{onset},

Sample	Site	Fraction / %	δ_{iso} / ppm	$\Delta\delta_{iso}$ / ppm	C_Q / MHz	η_Q
LSGP	Sc1	99.0	11.6	35.7	12.5	—
	Sc2	1.0	−42.6	—	6.1	0.65
LSGP-C-600	Sc1	99.4	8.7	38.3	11.4	0.52
	Sc2	0.6	−55.0	—	5.1	
LSGP-C-690	—	100	43.3	20.9	13.0	—
LSGP-C-832	Sc1	95.5	34.7		6.4	1.0
	Sc2	2.9	47.2		4.6	0.52
	Sc3	0.9	64.8		8.0	0.57
	Sc4	0.7	−49.6		4.4	0.62

TABLE 4 ^{45}Sc chemical shift values and quadrupolar parameters acquired from numerical deconvolution of the ^{45}Sc MAS NMR experimental spectra. Resonances deconvoluted by the Czjzek model have $\Delta\delta_{iso}$ values (full width at half maximum of a Gaussian distribution in δ_{iso}) but this analysis produces no η_Q value while resonances deconvoluted assuming first- and second-order effect of quadrupolar interaction on the Zeeman levels produce η_Q values but no $\Delta\delta_{iso}$ values. Estimated errors are ± 1% for the fractions, ±1 ppm for both δ_{iso} and $\Delta\delta_{iso}$, ±0.1 MHz for C_Q and ± 0.05 for η_Q

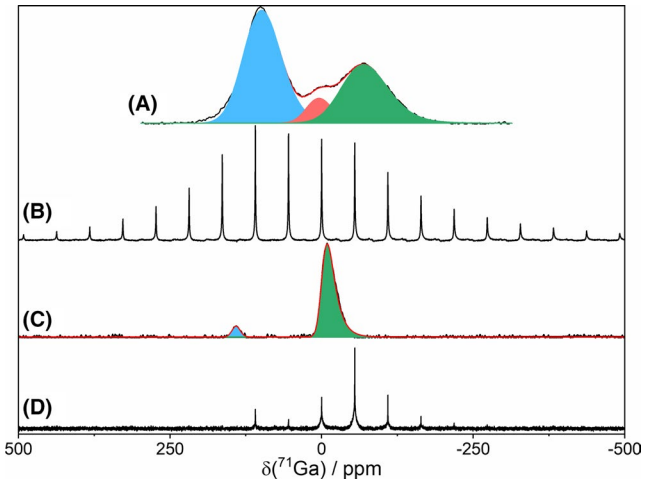

FIGURE 8 ^{71}Ga MAS (A,C) and QCPMG (B,D) NMR spectra of samples LGGP and LGGP-C-606 (black line) and their deconvolution (red curve in A). Four-, five-, and six-coordinated gallium resonances are highlighted in blue, red and green respectively in A and C. [Color figure can be viewed at wileyonlinelibrary.com]

reaching a constant plateau value at high temperature, corresponding to the fast motion regime. For sample LGGP-C-606, the ion dynamics are so fast on the NMR timescale (kHz) that the rigid lattice regime could not be reached within the experimentally accessible temperature range.

4 | DISCUSSION

From the X-ray powder patterns, one can see that substitution of Ge^{4+} by Ga^{3+} and Sc^{3+} was successful, although in the latter case a multiphase crystallization pattern was observed in the DSC analysis for LSGP precursor glass and some extra peaks were also observed in the diffraction pattern. As previously shown, the exact degree of Ge substitution x in the NASICON phase can be obtained from the ^{31}P MAS-NMR spectra using the expression[2,13,14,24]

$$\frac{M^{3+}}{Ge^{4+}} = \frac{4I_4 + 3I_3 + 2I_2 + I_1}{I_3 + 2I_2 + 3I_1 + 4I_0} = \frac{x}{2-x}, \quad (2)$$

where I_n refers to the fractional area of each $P^4_{(4\text{-}n)Ge,nM}$ signal component. Using the data shown in Table 3, values of $x = 0.53$ and 0.38 are calculated for LGGP-C-606 and LSGP-C-690, respectively. For samples LSGP-C-832 and LYGP-C-728, the situation is unclear from the solid-state NMR spectra, even though the small unit cell volume expansion of the NASICON structure observed by XRD (as shown in Table 2) suggests a substitution level of x well below 0.1. Overall, our data indicate successful substitution of Ge^{4+} by Ga^{3+} and Sc^{3+}, although the gallium substitution appears to be more efficient since all of the batched gallium content enters the NASICON structure in our samples. For the scandium-containing samples, higher crystallization temperatures appear to promote the crystallization of the $LiScP_2O_7$ phase, which has a structure similar to $LiGe_2(PO_4)_3$, where a scandium-centered octahedron is linked to tetrahedral phosphate units by corner-sharing oxygens.[39] R. Kahlaoui et.al.[33] studied the substitution of Ti^{4+} by Sc^{3+} in $Li_{1+x}Sc_xTi_{2-x}(PO_4)_3$ ($0 \le x \le 0.5$) and reported that the real value of x calculated from the ^{31}P MAS NMR data starts to deviate from the nominal value for $x_{nominal} = 0.2$. In addition, the authors found that the real value for $x_{nominal} = 0.5$ is 0.33, which is in good agreement with the value of 0.38 found here for sample LSGP-C-690. The substitution of Ge^{4+} by Y^{3+} was not achieved as shown by the X-ray powder pattern and the ^{31}P MAS NMR spectra. Arbi et.al.[26] reported the substitution of Ti^{4+} by R^{3+} (R = Al, Ga, Sc, In, Y) in $Li_{1.2}Ti_{1.8}R_{0.2}(PO_4)_3$ glass-ceramics and showed that the Y^{3+} substitution was indeed the only one that did not work. In the case of gallium and scandium, they observed that the efficiency of the substitution was the same for both trivalent ions ($x = 0.16$ and 0.18 for R = Ga and Sc respectively). However, although basically all gallium and scandium enter the NASICON structure of $LiTi_2(PO_4)_3$ in their case, one should note that the authors used a lower content of trivalent ions than the ones reported in the present contribution.

TABLE 5 ^{71}Ga chemical shifts and quadrupolar parameters found by deconvolution of the experimental ^{71}Ga MAS NMR spectra. Estimated errors are ± 1% for the fractions, ±1 ppm for both δ_{iso} and $\Delta\delta_{iso}$, and ± 0.1 MHz for C_Q

Sample		Fraction /%	δ_{iso} /ppm	$\Delta\delta_{iso}$ /ppm	C_Q /MHz
LGGP	Ga_{IV}	55.7	117.2	63.5	4.9
	Ga_V	8.5	17.6	43.1	4.2
	Ga_{VI}	35.8	−44.0	75.0	5.9
LGGP-C-606	Ga_{IV}	6.3	143.6	15.1	1.7
	Ga_{VI}	93.7	−3.5	14.1	3.6

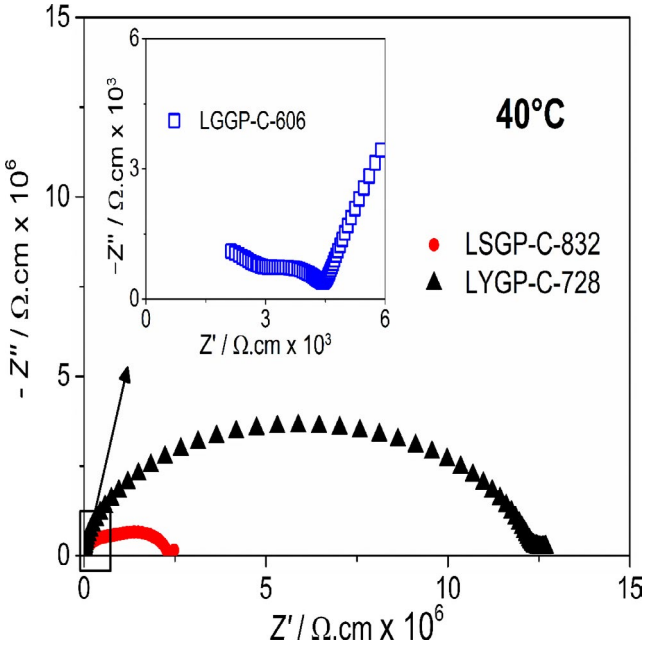

FIGURE 9 Impedance plots of samples LGGP-C-606, LSGP-C-832, and LYGP-C-728 at 40°C. [Color figure can be viewed at wileyonlinelibrary.com]

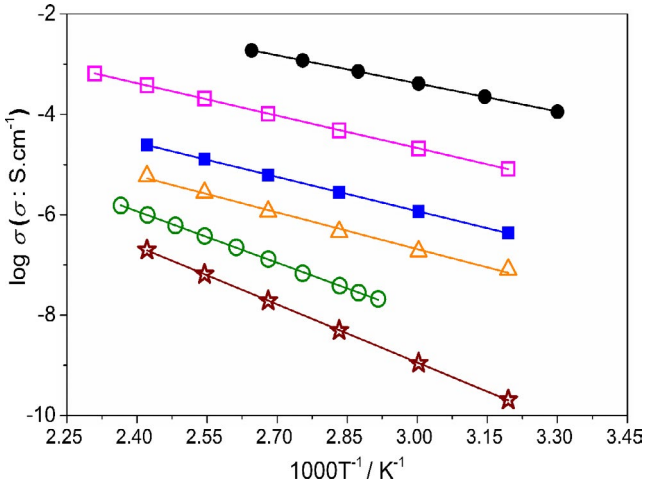

FIGURE 10 Arrhenius plots for the overall ionic conductivity of samples LGGP-C-606 (●), LSGP-C-690 (□), LSGP-C-832 (■), LYGP-C-728 (Δ), $LiGe_2(PO_4)_3$ (○) (Ref. [21]), and LSGP-C-600 (☆), Solid lines represent the linear fitting of experimental data. [Color figure can be viewed at wileyonlinelibrary.com]

Unsuccessful Y^{3+} substitution into the $Li_{1+x}Y_xGe_{2-x}(PO_4)_3$ system with $x = 0.2$ and 0.4 was also reported by Yamamoto et al.[25]

The success of the gallium substitution is also shown by ^{71}Ga MAS NMR, where almost 94% of the ^{71}Ga MAS NMR spectral area is due to six-coordinated gallium on the Ge site. The other 6% are found in four-coordinated sites that might be due to substitution of phosphorus by gallium in the tetrahedral site (formation of GaO_4^- ions in the anionic sublattice) or crystallization of $GaPO_4$. The first type of substitution was proposed in the case of some samples in the $Li_{1+x}Al_xM_{2-x}(PO_4)_3$ (M = Ti and Ge) system, where the authors had no evidence of crystallization of $AlPO_4$.[40,41] The latter, on the other hand, was reported for $Li_{1+x}Ga_xGe_{2-x}(PO_4)_3$ for $x \geq 0.4$ where the crystallization of $GaPO_4$ was observed by X-ray powder diffraction, ^{31}P MAS NMR, and ^{71}Ga MAS NMR.[24] As we found no evidence of the crystallization of $GaPO_4$ in our data, the only explanation may be the existence of GaO_4^- units substituting in the anionic sublattice. This could also explain why the chemical shift value of the four-coordinated gallium resonance in Figure 7 is more positive (142.8 ppm for LGGP-C-606) than the chemical shifts reported for both $GaPO_4$ structures (100.3 ppm for $GaPO_4$ in the quartz and 118.0 ppm for $GaPO_4$ in the cristobalite polymorphs).[42]

The interpretation of the ^{45}Sc MAS NMR spectra in terms of coordination number is more complicated because in the case of six-coordinated Sc, the chemical shift values can vary by more than 100 ppm.[29] However, literature data indicate a tendency of six-coordinated scandium toward positive chemical shift values and of eight-coordinated scandium toward negative chemical shift values.[29,43] Based on the correlation suggested by Bräuniger et al.[43] for a limited set of Sc compounds ($ScPO_4$, Sc_2O_3, ScOF, $CaSc_2O_4$, and $Li_3Sc(BO_3)_2$) with coordination numbers of 6, 7, and 8, it may be tempting to assign the resonance in the glassy state to seven-coordinated scandium. On the other hand, comparison with other data on crystalline scandium phosphates[29] suggests that scandium is more likely to be six-coordinated in the glasses. For sample LSGP-C-690, the Czjzek analysis indicates an average chemical shift of 43.3 ppm which is consistent with octahedrally coordinated Sc. The distribution width of 20.9 ppm reflects the intrinsic disorder in the NASICON phase, which is expected based on the random substitution of Ge by Sc.

The highest overall room temperature conductivity achieved for our samples is 1.1×10^{-4} S/cm for the essentially phase-pure sample LGGP-C-606. The corresponding

Sample	E_a / eV	σ_{RT} / S.cm^{-1}	$\log_{10}(\sigma_0)$, $[\sigma_0]$ = S.cm^{-1}
$LiGe_2(PO_4)_3$	0.674	9.77×10^{-10}	2.21
LGGP-C-606	0.369 ± 0.001	$(1.1 \pm 0.1) \times 10^{-4}$	2.20 ± 0.01
LSGP-C-600	0.765 ± 0.001	$(7.9 \pm 0.1) \times 10^{-11}$	2.66 ± 0.01
LSGP-C-690	0.427 ± 0.002	$(4.8 \pm 0.1) \times 10^{-6}$	1.79 ± 0.02
LSGP-C-832	0.450 ± 0.001	$(2.5 \pm 0.1) \times 10^{-7}$	0.88 ± 0.01
LYGP-C-728	0.483 ± 0.001	$(4.9 \pm 0.1) \times 10^{-8}$	0.62 ± 0.01

TABLE 6 Activation energy (E_a), total conductivity at room temperature (σ_{RT}), and pre-exponential factor (σ_0) acquired by assuming an Arrhenius behavior of the overall conductivity $\sigma(T)$. Data for $LiGe_2(PO_4)_3$ were taken from Ref. [21]

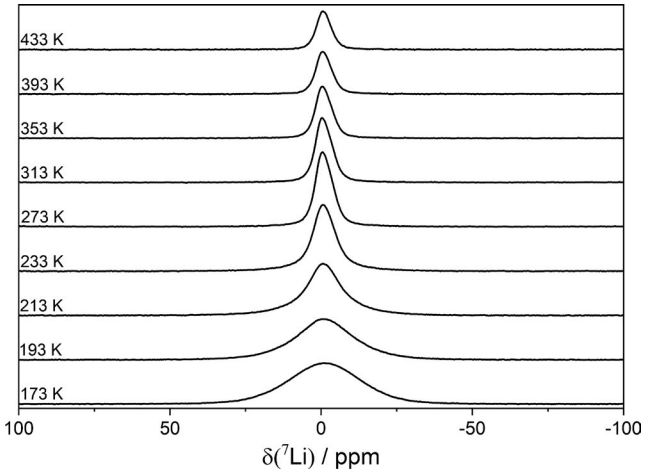

FIGURE 11 ^{7}Li static NMR spectra of sample LGGP-C-606 at selected temperatures between 160 and 440 K.

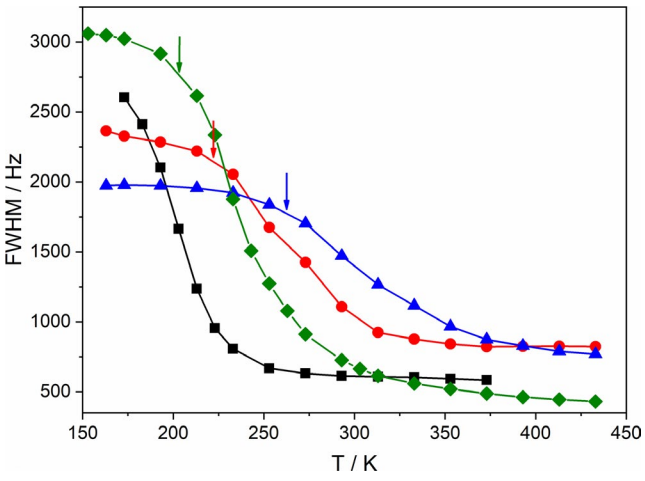

FIGURE 12 Temperature dependence of the full width at half maximum (FWHM) of the ^{7}Li NMR spectra for samples LGGP-C-606 (■), LSGP-C-690 (♦), LSGP-C-832 (●), and LYGP-C-728 (▲). Solid curves are guides to the eye. Arrows mark T_{onset} temperatures used to estimate the activation energies from the Waugh-Fedin empirical formula (see text). [Color figure can be viewed at wileyonlinelibrary.com]

activation energy determined from an Arrhenius analysis of temperature-dependent conductivity measurement is 0.37 eV, which is comparable to the value of 0.41 eV reported by Zhang et al for a sample with nominal Gallium content of $x = 0.6$.[24] Samples LSGP-C-690 and LSGP-C-832 show an overall room temperature conductivity of 4.8×10^{-6} and 2.5×10^{-7} S/cm, respectively. The former can be explained by partial crystallization of the $Li_{1.38}Sc_{0.38}Ge_{1.62}(PO_4)_3$ NASICON phase while the latter can be explained on the basis of the crystallization of $LiScP_2O_7$, which has a reported ionic conductivity at room temperature of 4×10^{-7} S/cm.[39] In the case of the LSGP-C-600 sample, the lowest ionic conductivity is expected, as the precursor glasses of NASICON glass-ceramics are usually more resistive than its respective crystallized samples.[8,44] In those glass ceramics in which no cation substitution takes place because the trivalent species forms non-ion conducting crystalline components such as YPO_4, one would generally expect the ionic conductivity to be lower than in $LiGe_2(PO_4)_3$. In contrast, for sample LYGP-C-728, the overall room temperature conductivity is found to be two orders of magnitude higher than the reported one for the unsubstituted NASICON ($LiGe_2(PO_4)_3$). A similarly surprising result was reported by Vizgalov et al[45] who showed that the addition of Y_2O_3 in the glass batch of $Li_{1.5}Al_{0.5}Ge_{1.5}(PO_4)_3$, resulted in the crystallization of YPO_4 upon thermal treatment. They also evidenced an increase in the ionic conductivity compared to the unsubstituted LGP NASICON phase and they attributed this enhancement to the presence of YPO_4 microcrystals, which promote better contact between the NASICON grains. Likewise, Yamamoto et al[26] suggested that the $Li_4P_2O_7$ secondary phase also contributes to improved grain contacts in the $LiGe_2(PO_4)_3$ NASICON compound. An increase by one and a half orders of magnitude in the ionic conductivity of LGP samples was observed. Similar behavior was also reported by Aono et al[46] in $LiTi_2(PO_4)_3$ (LTP) ceramics-containing titanium in place of germanium. Again, an improvement in the contact area between grains due to the formation of $Li_4P_2O_7$ was attributed to be responsible for the increase in the ionic conductivity of LTP samples.

From the temperature dependence of the FWHM of the static ^{7}Li NMR spectra, one can estimate the activation energy of the faster lithium-ion using the empirical expression proposed by Waugh and Fedin:

$$E_A \approx 1.617 \times 10^{-3} T_{onset} \quad (3)$$

From this expression, activation energies were estimated as (0.33 ± 0.01) eV for sample LSGP-C-690, (0.36 ± 0.01) eV for sample LSGP-C-832, and (0.43 ± 0.01) eV for sample LYGP-C-728. It was not possible to estimate the activation energy for sample LGGP-C-606 since T_{onset} could not be determined for this sample, as the low-temperature plateau could not be reached due to hardware limitations (Figure 12). As frequently reported, the activation energies deduced from NMR lineshape analysis are significantly lower than those determined by electrical conductivity measurements, even though the compositional trends are the same.[47] The discrepancy most likely arises because the two techniques probe into ionic motion on different length scales.[48] In addition, there is most likely a distribution of mobilities and activation energies, resulting in a distribution of onset temperatures. Thus, by identifying those temperatures at which the linewidths get noticeably reduced, the Waugh-Fedin method tends to emphasize the contribution of those ions that are most mobile.

5 | CONCLUSION

Substitution of Ge^{4+} by Ga^{3+}, Sc^{3+}, and Y^{3+} in the $LiGe_2(PO_4)_3$ NASICON phase was attempted using the glass-ceramic route. The results show that phase-pure $Li_{1.5}Ga_{0.5}Ge_{1.5}(PO_4)_3$ could be obtained as also reported recently.[24] Substitution by Sc^{3+} was achieved for the samples heat treated at 690°C for 1h (LSGP-C-690), although no phase-pure samples were obtained. No indication of any substitution of Ge^{4+} by Y^{3+} was observed in the NMR data. The different degrees of substitution can be explained on the basis of the differences in the ionic radii. While Ga^{3+} ions ($r = 62$ pm) can still be accommodated substituting for Ge^{4+} ($r = 53$ pm), those of Sc^{3+}($r = 74.5$ pm) and Y^{3+} (90 pm) are significantly larger. Still, the possibility of at least partial substitution documented for Sc^{3+} in this study reflects an impressive tolerance of the NASICON lattice for ionic size mismatch on the Ge sites. The highest room ionic conductivity (1.1×10^{-4} $(\Omega.cm)^{-1}$) was achieved for Ga-substituted samples, which presented the NASICON as a single phase.

ACKNOWLEDGMENTS

The authors acknowledge the financial support of Fundação de Amparo a Pesquisa do Estado de São Paulo (FAPESP) through grant number 2013/00793-6 (Center for Research, Technology, and Education on Vitreous Materials – CeRTEV). IDA Silva acknowledges the financial support from FAPESP grant 2017/17800-0. The Coordenação de Aperfeiçoamento de Pessoal de Nível Superior - (CAPES), Brazil, Finance Code 001, is also acknowledged.

ORCID

Igor d'Anciães Almeida Silva https://orcid.org/0000-0001-8830-7661

Ana Candida M. Rodrigues https://orcid.org/0000-0003-1689-796X

Hellmut Eckert https://orcid.org/0000-0002-6536-0117

REFERENCES

1. The Nobel Prize in Chemistry 2019. NobelPrize.org. Nobel Media AB 2019. Mon 28 Oct 2019. https://www.nobelprize.org/prizes/chemistry/2019/summary/.
2. Eckert H, Rodrigues ACM. Ion-conducting glass-ceramics for energy storage applications. MRS Bull. 2017;42:206–12.
3. Bachman JC, Muy S, Grimaud A, Chang H-H, Pour N, Lux SF, et al. Inorganic solid-state electrolytes for lithium batteries: mechanisms and properties governing ion conduction. Chem Rev. 2016;116:140–62.
4. Anantharamulu N, Koteswara Rao K, Rambabu G, Vijaya Kumar B, Radha V, Vithal M. A wide-ranging review on NASICON type materials. J Mater Sci. 2011;46(9):2821–37.
5. Fergus JW. Ceramic and polymeric solid electrolytes for lithium ion batteries. J Power Sources. 2010;195:4554–96.
6. Fu J. Lithium ion conductive glass-ceramics. US Patent 5,702,995. 1997. [patent].
7. Fu J. Fast Li^+ ion conducting glass-ceramics in the system Li_2O–Al_2O_3–GeO_2–P_2O_5. Solid State Ionics. 1997;104:191–4.
8. Fu J. Superionic conductivity of glass-ceramics in the system Li_2O–Al_2O_3–TiO_2–P_2O_5. Solid State Ionics. 1997;96:195–200.
9. Fu J. Fast Li^+ ion conducting glass-ceramics in the system Li_2O – Al_2O_3 – TiO_2 – SiO_2 – P_2O_5. J Am Ceram Soc. 1997;80(7):1901–3.
10. París MA, Sanz J. Structural changes in the compounds $LiM_2IV(PO_4)_3$ (MIV = Ge, Ti, Sn, and Hf) as followed by 31P and 7Li NMR. Phys Rev B 1997;55(21):14270–8.
11. Shannon RD. Revised effective ionic radii and systematic studies on interatomic distances in halides and chalcogenides. Acta Cryst. 1976;A32:751–67.
12. Cruz AM, Ferreira EB, Rodrigues ACM. Controlled crystallization and ionic conductivity of a nanostructured $LiAlGePO_4$ glass-ceramics. J Non-Cryst Solids. 2009;335:2295–301.
13. Schröder C, Ren J, Rodrigues ACM, Eckert H. Glass-to-crystal transition in $Li_{1+x}Al_xGe_{2-x}(PO_4)_3$: structural aspects studied by solid-state NMR. J Phys Chem C. 2014;118:9400–11.
14. Arbi K, Bucheli JR, Sanz J. High lithium ion conducting slid electrolytes based on NASICON $Li_{1+x}Al_xM_{2-x}(PO_4)_3$ materials (M = Ti, Ge and $0 \le x \le 0.5$). J Eur Ceram Soc. 2015;35:1477–84.
15. Liu Z, Venkatachalam S, van Wüllen L. Structure, phase separation and Li dynamics in sol-gel-derived $Li_{1+x}Al_xGe_{2-x}(PO_4)_3$. Solid State Ionics. 2015;276:47–55.
16. Hayamizu K, Seki S. Long-range Li ion diffusion in NASICON-type $Li_{1.5}Al_{0.5}Ge_{1.5}(PO_4)_3$ (LAGP) studied by ^7Li pulsed-gradient spin-echo NMR. Phys Chem Chem Phys. 2017;19:23483–91.
17. Safanama D, Sharma N, Rao RP, Brand HEA, Adams S. Structural evolution of NASICON-type $Li_{1+x}Al_xGe_{2-x}(PO_4)_3$ using *in-situ* synchrotron X-ray powder diffraction. J Mater Chem A. 2016;4:7718–26.
18. Meesala Y, Chen CY, Jena A, Liao YK, Hu SF, Chang H, et al. All-solid-state Li-ion battery using $Li_{1.5}Al_{0.5}Ge_{1.5}(PO_4)_3$ as electrolyte without polymer interface adhesion. J Phys Chem C. 2018;122:14383–9.
19. Zhang Z, Chen S, Yang J, Liu G, Yao X, Cui P, et al. Stable cycling of all-solid-state lithium battery with surface amorphized $Li_{1.5}Al_{0.5}Ge_{1.5}(PO_4)_3$ electrolyte and lithium anode. Electrochim Acta. 2019;297:281–7.

20. Zhang K, Mu S, Liu W, Zhu D, Ding Z, Chen Y. A flexible NASICON-type composite electrolyte for lithium-oxygen/air battery. Ionics. 2019;25:25–33.
21. Santagneli SH, Baldacim HVA, Ribeiro SJL, Kundu S, Rodrigues ACM, Doerenkamp C, EckertH Preparation, structural characterization, and electrical conductivity of highly ion-conducting glass and glass ceramics in the system $Li_{1+x}Al_xSn_yGe_{2-(x+y)}(PO_4)_3$. J Phys Chem C. 2016;120:14556–67.
22. Francisco BE, Stoldt CR, M'Peko JC. Lithium-ion trapping from local structural distortion in sodium super ionic conductor (NASICON) electrolytes. Chem Mater. 2014;26:4741–9.
23. Nuernberg RB, Rodrigues ACM. A new NASICON lithium ion-conducting glass-ceramic of the $Li_{1+x}Cr_x(Ge_yTi_{1-y})_{2-x}(PO_4)_3$ system. Solid State Ionics. 2017;301:1–9.
24. Zhang Z, Hu L, Tao H, Ren J. Li super ionic conducting glasses and glass ceramics in the $Li_{1+x}Ga_xGe_{2-x}(PO_4)_3$ system: Solid state nuclear magnetic resonance and electrical conductivity study. J Power Sources. 2019;442:227169.
25. Arbi K, Lazarraga MG, Ben Hassen Chehimi D, Ayadi-Trabelsi M, Rojo JM, Sanz J. Lithium mobility in $Li_{1.2}Ti_{1.8}R_{0.2}(PO_4)_3$ compounds (R = Al, Ga, Sc, In) as followed by NMR and impedance spectroscopy. Chem Mater. 2004;16:255–62.
26. Yamamoto H, Tabuchi M, Takeuchi T, Kageyama H, Nakamura O. Ionic conductivity enhancement in $LiGe_2(PO_4)_3$ solid electrolyte. J Power Sources. 1997;68:397–401.
27. Lutterotti L, Bortolotti M, Ischia G, Lonardelli I, Wenk HR. Rietveld texture analysis from diffraction images. Z Kristallogr Suppl. 2007;26:125–30.
28. Larsen FH, Jakobsen HJ, Ellis PD, Nielsen NC. Sensitivity-enhanced quadrupolar-echo of half-integer quadrupolar nuclei. Magnitude and relative orientation of chemical shielding and quadrupolar coupling tensors. J Phys Chem A. 1997;101:8597–606.
29. Mohr D. Solid State NMR Studies of Scandium Compounds, Doctoral Dissertation, WWU Münster, 2010.
30. Han OH, Timken HKC, Oldfield E. Solid-state, "magic-angle" sample spinning nuclear magnetic resonance spectroscopic studies of group III-V (13–15) semiconductors. J Phys Chem. 1988;89(10):6046–52.
31. Massiot D, Fayon F, Capron M, et al. Modeling one and two-dimensional solid state NMR spectra. Magn Reson Chem. 2002;40:70–6.
32. Alami M, Brochu R, Soubeyroux JL, Gravereau P, Le Flem G, Hagenmueller P. Structure and thermal expansion of $LiGe_2(PO_4)_3$. J Solid State Chem. 1991;90:185–93.
33. Kahlaoui R, Arbi K, Sobrados I, Jimenez R, Sanz J, Ternane R. Cation miscibility and lithium mobility in NASICON $Li_{1+x}Ti_{2-x}Sc_x(PO_4)_3$ ($0 \le x \le 0.5$) series: A combined NMR and impedance study. Inorg Chem. 2017;56:1216–24.
34. Nalin M, Ribeiro SJL, Messaddeq Y, Schneider J, Donoso P. Scandium fluorophosphate glasses: a structural approach. C. R. Chimie. 2002;5(12):915–20.
35. Palke AC, Stebbins JF. Paramagnetic interactions in the ^{31}P NMR spectroscopy of rare earth element orthophosphate ($REPO_4$, monazite/xenotime) solid solutions. Am Miner. 2011;96(8–9):1343–53.
36. d'Espinose de Lacaillerie JB, Fretigny C, Massiot D. NMR spectra of quadrupolar nuclei in distorted solids: The Czjzek model. J Magn Reson. 2008;192:244–51.
37. Ren J, Eckert H. Intermediate role of gallium in oxidic glasses: solid state NMR structural studies of the Ga_2O_3–$NaPO_3$ system. J Phys Chem C. 2014;118:15386–403.
38. Massiot D, Farnan I, Gautier N, Trumeau D, Trokiner A, Coutures JP. ^{71}Ga and ^{69}Ga nuclear magnetic resonance study of β-Ga_2O_3: Resolution of four- and six-fold coordinated Ga sites in static conditions. Solid State Nucl Magn. Reson. 1995;4:241–8.
39. Vītinš G, Kanepe Z, Vītinš A, Ronis J, Dindūne A, Lūsis A. Structural and conductivity studies in $LiFeP_2O_7$, $LiScP_2O_7$, and $NaScP_2O_7$. J Solid State Electrochem. 2000;4:146–52.
40. Forsyth M, Wong S, Nairn KM, Best AS, Newman PJ, MacFarlane DR. NMR studies of modified Nasicon-like, lithium conducting solid electrolytes. Solid State Ionics. 1999;124:213–9.
41. Maldonado-Manso P, Martín-Sedeño MC, Bruque S, Sanz J, Losilla ER. Unexpected cationic distribution in tetrahedral/octahedral sites in nominal $Li_{1+x}Al_xGe_{2-x}(PO_4)_3$ NASICON series. Solid State Ionics. 2007;178:43–52.
42. Massiot D, Vosegaard T, Magneron N, Trumeau D, Montouillout V, Berthet P, et al. ^{71}Ga NMR of reference Ga_{IV}, Ga_V, and Ga_{VI} compounds by MAS and QPASS, extension of gallium/aluminum NMR parameter correlation. Solid State Nucl Magn. Reson. 1999;15:159–69.
43. Bräuniger T, Hofmann AJ, Moudrakovski IL, Hoch C, Schnick W. A ^{45}Sc-NMR and DFT study of crystalline scandium compounds. Solid State Sci. 2016;51:1–7.
44. Ortiz-Mosquera JF, Nieto-Muñoz AM, Rodrigues ACM. Precursor glass stability, microstructure and ionic conductivity of glass-ceramics from the $Na_{1+x}Al_xGe_{2-x}(PO_4)_3$ NASICON series. J Non-Cryst. Solids. 2019;513:36–43.
45. Vizgalov VA, Nestler T, Trusov LA, Bobrikov IA, Ivankov OI, Avdeev MV, et al. Enhancing lithium-ion conductivity in NASICON glass-ceramics by adding yttria. Cryst Eng Comm. 2018;20:1375–82.
46. Aono H, Sugimoto E, Sadaoka Y, Imanaka N, Adachi G. Ionic conductivity of solid electrolytes based on lithium titanium phosphate. J Electrochem Soc. 1990;137(4):1023–7.
47. Storek M, Böhmer R, Martin SW, Larink D, Eckert H. NMR and conductivity studies of the mixed glass-former effect in lithium borophosphate glasses. J Chem Phys. 2012;137:124507.
48. Böhmer R, Jeffrey KR, Vogel M. Solid-state Li NMR with applications to the translational dynamics in ion conductors. Prog Nucl Magn Reson Spectrosc. 2007;50:87–174.

How to cite this article: d'Anciães Almeida Silva I, Nieto-Muñoz AM, Rodrigues ACM, Eckert H. Structure and lithium-ion mobility in $Li_{1.5}M_{0.5}Ge_{1.5}(PO_4)_3$ (M = Ga, Sc, Y) NASICON glass-ceramics. *J Am Ceram Soc*. 2020;103:4002–4012. https://doi.org/10.1111/jace.16998